processes

MDPI

Article

Molecular Dynamics Simulation of Femtosecond Laser Ablation of $Cu_{50}Zr_{50}$ Metallic Glass Based on Two-Temperature Model

Jingxiang Xu [1,*], Dengke Xue [1], Oleg Gaidai [1], Yang Wang [2] and Shaolin Xu [3]

[1] College of Engineering Science and Technology, Shanghai Ocean University, Shanghai 201306, China; m200601296@st.shou.edu.cn (D.X.); o_gaidai@just.edu.cn (O.G.)
[2] Research Institute of Frontier Science, Southwest Jiaotong University, Chengdu 610031, China; yang.wang@swjtu.edu.cn
[3] Department of Mechanical and Energy Engineering, Southern University of Science and Technology, Shenzhen 518055, China; xusl@sustech.edu.cn
* Correspondence: jxxu@shou.edu.cn; Tel.: +86-21-61900801

Abstract: Femtosecond laser machining, characterized by a small heat-affected zone, high precision, and non-contact operation, is ideal for processing metallic glasses. In this study, we employed a simulation method that combines the two-temperature model with molecular dynamics to investigate the effects of fluence and pulse duration on the femtosecond laser ablation of $Cu_{50}Zr_{50}$ metallic glass. Our results showed that the ablation threshold of the target material was 84 mJ/cm^2 at a pulse duration of 100 fs. As the pulse durations increased, the maximum electron temperature at the same position on the target surface decreased, while the electron–lattice temperature coupling time showed no significant difference. As the absorbed fluence increased, the maximum electron temperature at the same position on the target surface increased, while the electron–lattice temperature coupling time became shorter. The surface ablation of the target material was mainly induced by phenomena such as melting, spallation, and phase explosion caused by femtosecond laser irradiation. Overall, our findings provide valuable insights for optimizing the femtosecond laser ablation process for metallic glasses.

Keywords: femtosecond laser; metallic glass; ablation; two-temperature model; molecular dynamics

check for updates

Citation: Xu, J.; Xue, D.; Gaidai, O.; Wang, Y.; Xu, S. Molecular Dynamics Simulation of Femtosecond Laser Ablation of $Cu_{50}Zr_{50}$ Metallic Glass Based on Two-Temperature Model. *Processes* **2023**, *11*, 1704. https://doi.org/10.3390/pr11061704

Academic Editors: Zejia Zhao, Guoqing Zhang and Wai Sze YIP

Received: 6 May 2023
Revised: 26 May 2023
Accepted: 31 May 2023
Published: 2 June 2023

Copyright: © 2023 by the authors. Licensee MDPI, Basel, Switzerland. This article is an open access article distributed under the terms and conditions of the Creative Commons Attribution (CC BY) license (https://creativecommons.org/licenses/by/4.0/).

1. Introduction

Metallic glasses, also known as amorphous alloys or liquid metals, are a unique material characterized by a disorderly arrangement of atoms [1]. Due to their unique atomic structure, they generally exhibit excellent mechanical properties, high elasticity, superplasticity in the supercooled liquid region, exceptional soft magnetic properties, corrosion resistance, and remarkable electrocatalytic performance [2]. Despite these favorable properties, metallic glasses become harder and more brittle under low-temperature conditions, show a highly viscous state in medium- to high-temperature conditions, and are susceptible to self-passivation, which results in the formation of a surface film that can easily denature due to crystallization or oxidation caused by thermal effects [3]. To overcome these limitations, Yao et al. [4] suggests that employing femtosecond laser ablation to process metallic glasses offers several benefits, such as a small heat-affected zone, perquisite precise ablation thresholds, and the ability to perform precise, non-crystallization processing of metallic glasses. The purpose of this article is to enhance our understanding of the mechanism behind the ablation process during the femtosecond laser machining of metallic glasses.

There is currently limited research on femtosecond laser ablation in metallic glass processing. Some research has been conducted experimentally. Sano et al. [5] first reported on the use of the femtosecond laser for ablating bulk metallic glass and studied the relationship between pulse energies and ablation depth in air. Wang et al. [6] conducted

micro-drilling and trenching studies on amorphous alloys using femtosecond laser ablation in air, proposing that femtosecond laser ablation has the potential to achieve the amorphous processing of metallic glasses. Ma et al. [7] further investigated the femtosecond laser ablation of metallic glass under different laser shots and fluence in the atmospheric environment and provided guidance for controlling the evolution of surface morphology induced by femtosecond laser pulse.

Researchers have conducted some studies in the computational aspect as well. The two-temperature model (TTM) [8] has been used to describe the evolution of electronic and lattice temperatures in the short-pulse laser ablation of metals. Molecular dynamics (MD) simulation has been used to investigate the various mechanisms involved in the ablation process, such as ablation mechanisms [9–11], laser-induced shock waves [12], and melting [13]. However, due to the short period of femtosecond laser pulses and the complex effects resulting from the overlapping of multiple processes, it is difficult to observe the evolution process through experimental means. TTM cannot observe changes in atomic structure, while MD lacks descriptions of electrons. Thus, the mechanism between the femtosecond laser and metallic glasses is not yet fully understood by these methods.

To conduct research in this field, many researchers employ the TTM-MD hybrid model. Most simulations focus on the interaction between femtosecond lasers and monometallic materials such as Cu [14], Al [15], Ni [16], and Au [17]. For metallic glasses, Marinier et al. [18] studied the ablation dynamics of CuZr metallic glass and crystal structure materials using a MD simulation combined with the TTM under femtosecond laser irradiation. Iabbaden et al. [19] also employed a hybrid TTM-MD model to investigate the structural evolution of crystalline CuZr alloys and amorphous alloys of the same compositions under ultrashort laser irradiation. However, they overlooked the structural evolution of metallic glasses under different femtosecond laser irradiation conditions, which could significantly guide practical processing. The related mechanisms involved in the femtosecond laser ablation of metallic glasses remain unclear, especially the impact of different laser parameters on the ablation of metallic glasses.

Our study employed a hybrid TTM-MD model to investigate the ablation process of $Cu_{50}Zr_{50}$ metallic glass with a single-pulse femtosecond laser of different fluence and pulse durations. The study discussed the structural evolution of the target under different laser conditions, the distribution of the maximum electron temperature of the target surface, the electron–lattice temperature coupling time, and the propagation of pressure waves. The study also determined the ablation threshold of $Cu_{50}Zr_{50}$ metallic glass, which helps to understand the mechanism between the femtosecond laser and metallic glasses, as well as promotes the application of the femtosecond laser in processing metallic glasses.

2. Computational Modeling

2.1. TTM-MD Method

The simulation is studied by the LAMMPS (Large-scale Atomic/Molecular Massively Parallel Simulator) software [20]. The TTM-MD method combines two schemes where electrons of laser excitation are treated as a continuum on a regular grid [16], and ions are modeled on a classical MD.

$$\boldsymbol{F}_{ion} = -\frac{\partial U}{\partial \boldsymbol{r}_{ion}} + \boldsymbol{F}_{langevin} - \frac{\nabla P_e}{n_{ion}} \tag{1}$$

$$C_e(T_e)\frac{\partial T_e}{\partial t} = \nabla(k_e(T_e)\nabla T_e) - g_p(T_e - T_{ion}) + \frac{I(t)e^{-\frac{x}{l_p}}}{l_p} \tag{2}$$

In Equation (1), $\boldsymbol{F}_{ion}$ is the total force acting on an ion, $\frac{\partial U}{\partial \boldsymbol{r}_{ion}}$ is the force due to interatomic interactions, $\boldsymbol{F}_{langevin}$ represents the force due to electron–phonon coupling, $\frac{\nabla P_e}{n_{ion}}$ is the blast force acting on ions because of electronic pressure gradient [21,22], and n_{ion} is the ionic density.

Equation (2) is a 1D heat diffusion equation with an external heat source in the x direction. In this equation, $C_e(T_e)$ is the electronic specific heat, $k_e(T_e)$ is the electronic thermal conductivity, and g_p is the coupling coefficient for the electron–ion interaction. T_e and T_{ion} are, respectively, the electronic and ionic temperature. For the $Cu_{50}Zr_{50}$ metallic glass, a free electron model is used as $C_e(T_e) = \gamma T_e$, where the electronic specific heat coefficient γ is available in [19]. When the simulation time t is shorter than the pulse duration τ, $I(t) = I_0$ and 0 otherwise. I_0 is the initial laser pulse intensity, and the absorbed laser fluence is defined as $F_{\text{abs}} = I_0 \cdot \tau \cdot l_p$ is the penetration depth of the laser energy deposition.

The electronic thermal conductivity $k_e(T_e)$ is determined from Equation (3), by assuming it is simply proportional to the electron heat capacity $C_e(T_e)$,

$$k_e(T_e) = D_e \rho_e C_e(T_e) \tag{3}$$

where D_e is the electronic thermal diffusion coefficient and ρ_e is the number density of electrons. Moreover, the coupling constant for the electron–ion interaction g_p is given by:

$$g_p = \frac{3Nk_B\gamma_p}{\Delta V m} \tag{4}$$

where k_B is the Boltzmann's constant, m is the atomic mass, and ΔV and N represent the volume of the electronic grid cell and the total number of atoms inside each cell, respectively. g_p is considered as constant in this model.

The values of the parameters used in the TTM-MD method are shown in Table 1. The density of our prepared $Cu_{50}Zr_{50}$ sample was 7.14 g/cm^3, while that of the sample prepared by Iabbaden et al. [19] was 7.18 g/cm^3. This difference falls within an acceptable range.

Table 1. The input parameters for TTM-MD simulations of $Cu_{50}Zr_{50}$ metallic glass.

Physical Properties	Unit	Value
density ρ_0	g·cm^{-3}	7.14
electron–phonon factor g_p	10^{17} W·m^{-3}·K^{-1}	1.00 [18]
specific heat constant γ	J·m^{-3}·K^{-2}	321.30 [18]
electronic thermal conductivity k_e	W·m^{-1}·K^{-1}	3.85 [23]
electronic thermal diffusion D_e	10^{-5} m^2·s^{-1}	3.98 [19]
depth l_p	nm	14.30 [19]

2.2. Computational Details

This study focused on the $Cu_{50}Zr_{50}$ metallic glass due to its favorable amorphous-forming ability. The potential function utilized in this research was fitted by Mendelev et al. [24] based on the Finnis–Sinclair embedded atom model potential (EAM/FS) [25,26]. The NPT ensemble is a simulation technique where the number of particles, temperature, and pressure are kept constant, while the volume can vary. This constant pressure and temperature make the NPT ensemble suitable for simulating systems in contact with an environment with a fluctuating pressure and temperature. On the other hand, the NVE ensemble refers to a simulation technique where the number of particles, volume, and energy are kept constant while the temperature can vary. The NVE ensemble is particularly useful for systems that are isolated and do not exchange energy with their surroundings.

The $Cu_{50}Zr_{50}$ metallic glass sample was prepared using a melting and quenching simulation [27,28]. Initially, the $Cu_{50}Zr_{50}$ binary alloy sample with equal numbers of Cu and Zr atoms was generated using LAMMPS commands. Then, the sample was subjected to a 200 ps relaxation under the NPT ensemble with periodic boundary conditions and a temperature of 300 K. Subsequently, the sample was heated at a rate of 50 K/ps from 300 K to 2500 K to melt it. After heating the sample for 40 ps at 2500 K, the temperature was instantaneously quenched to 300 K within 25 ps. Finally, the sample was relaxed for approximately 100 ps under the NPT and NVE ensembles, with a relaxation temperature of

300 K, zero relaxation pressure, and a time step of 0.001 ps. As a result, a $Cu_{50}Zr_{50}$ metallic glass sample was obtained, with a size of 644.9 nm × 4.3 nm × 4.3 nm and composed of approximately 660,000 atoms, as displayed in Figure 1. The relaxation and laser ablation MD simulation processes both use microcanonical ensemble (NVE).

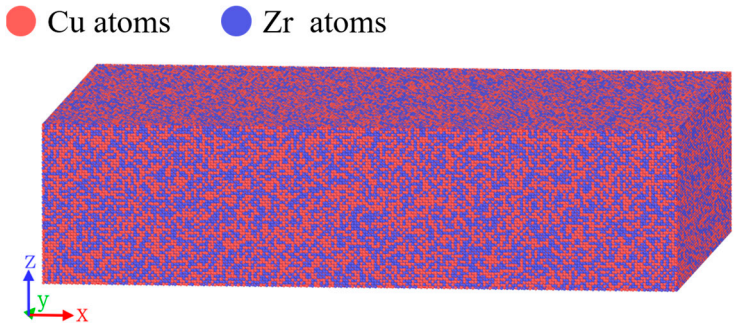

Figure 1. The substrate of the model (the Cu atoms are colored in red and the Zr atoms are colored in blue).

Figure 2 depicts a schematic model of the femtosecond laser ablation of $Cu_{50}Zr_{50}$ metallic glass. Upon being subjected to laser irradiation, the material absorbs the laser energy and undergoes thermal expansion or even ablation. Therefore, in constructing the simulation box, a vacuum layer was added to the upper surface of the target to prevent atoms from escaping the simulation box during the simulation process.

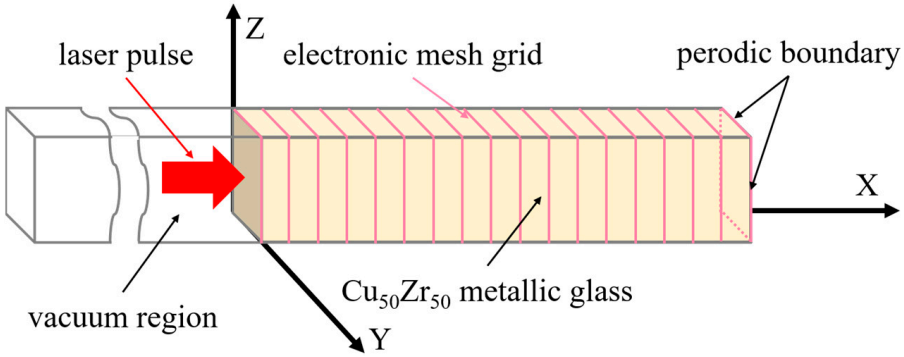

Figure 2. Simulation setup geometry used to model ultrafast laser pulse interaction in $Cu_{50}Zr_{50}$ metallic glass using TTM-MD simulations.

The heat diffusion Equation (2) is solved numerically on a 200 × 1 × 1 regular electronic cubic mesh, as shown in Figure 2. A step function $dx \approx 5$ nm is used for the T_e variation. Here, periodic boundary conditions are set in the y and z lateral directions and free boundaries are imposed following the laser shot $x = [0]$. The target irradiated by the femtosecond laser generates a pressure wave propagating towards the surface and into the target [29,30]. To avoid reflection of the pressure wave at the bottom of the target, we define non-reflecting boundary conditions composed of a viscous damping region [31–33] with a 100 nm in the x direction. A damping factor $\gamma_{damp} = 0.0025$ eV·ps·Å^{-2} [19] is used in this work in all simulations. The simulation is a regular MD run in the NVE ensemble after the laser pulse irradiation is completed.

To facilitate the simulation, we made some assumptions. These assumptions relate to the variables included in the simulation, the chosen force field, the simulation time step, and any other factors that may impact the accuracy and validity of the simulation results. Specifically, the assumptions of our proposed simulation include:

1. The model assumes that the interactions between atoms can be accurately represented by our chosen force field.

2. The model assumes the availability of accurate and reliable parameters to set up the force field.
3. The model assumes that the simulation time step is small enough to capture the dynamics of the system under investigation.
4. The model assumes that the simulation is conducted in a vacuum environment and heat exchange with the surroundings is neglected.
5. The model assumes that all of the laser energy is absorbed by the target and the reflectivity is zero.

3. Results

3.1. Ablation Threshold

When irradiated by the femtosecond laser, targets can undergo irreversible and permanent damage on their surfaces if the laser pulse parameters satisfy certain conditions, such as certain pulse duration and intensive enough laser fluence. Specifically, the surface of the target will be removed, and the minimum fluence that is required to achieve this kind of damage is known as the ablation threshold [18]. In our research, we determined the ablation threshold by gradually increasing the laser fluences. This method allowed for the determination of the specific energy requirements for ablation initiation in the target material and was chosen for its precision and reliability in determining the ablation threshold. Specifically, we determined the ablation threshold of the $Cu_{50}Zr_{50}$ metallic glass target material by incrementally increasing the laser fluence in 2 mJ/cm^2 intervals, with a baseline of 80 mJ/cm^2. We studied the results of the interaction between a femtosecond laser with a pulse duration of 100 fs and an absorbed fluence (80 + 2N, N = 0, 1, 2) mJ/cm^2 with the target material. The laser incidence direction was from left to right, and snapshots of the target at different times are shown in Figure 3.

From Figure 3a,b, it can be observed that the target surface expands significantly in the 0~40 ps time range after being irradiated by the laser pulse. During the 60–100 ps time range, the target surface remains in an expanded state but the target does not disintegrate, indicating that the ablation threshold of the target material is greater than 82 mJ/cm^2. In Figure 3c, at 20 ps, the target surface expands; and at 40 ps, a bubble appears at the position of x = 0 nm and the target expands. During the 60~100 ps time range, the target disintegrates due to the expansion of the bubble. The surface of the target is removed, and irreversible damage occurs. Therefore, the ablation threshold of the $Cu_{50}Zr_{50}$ metallic glass target material at a pulse duration of 100 fs is 84 mJ/cm^2. Hu et al. [34] predicted the damage threshold of the Cu50Zr50 amorphous alloy to be between 80 mJ/cm^2 and 120 mJ/cm^2. Further, we determined the ablation threshold to be within this range.

A comparison of Figure 4a,b indicates that the pressure within the target continuously propagates deeper, and its peak value gradually decreases over time. In Figure 4a, the pressure values remain relatively constant within the target material between x = 0~50 nm. Conversely, in Figure 4b, at the same position within the target, the pressure reaches its maximum value at 20 ps, subsequently decreasing. This variation suggests that there is a change in the stress state at the surface of the target material between 20~40 ps. The fracture mechanism of $Cu_{50}Zr_{50}$ metallic glass in Figure 3c was caused by the pressure induced by the femtosecond laser. At lower laser fluences (80 mJ/cm^2), the lattice temperature of the target material is not high enough and the tension near the surface is relatively small. As a result, only the expansion of the target material can be observed in the atomic structures shown in Figure 3a,b. When the laser fluence increases to 84 mJ/cm^2, more energy is absorbed at the surface of the target material, causing cavitation, which corresponds to breakage in Figure 3c. In Figure 4b, the tension near the surface decreases after 20 ps because it is "absorbed" by the cavities that ultimately lead to breakage (ablation).

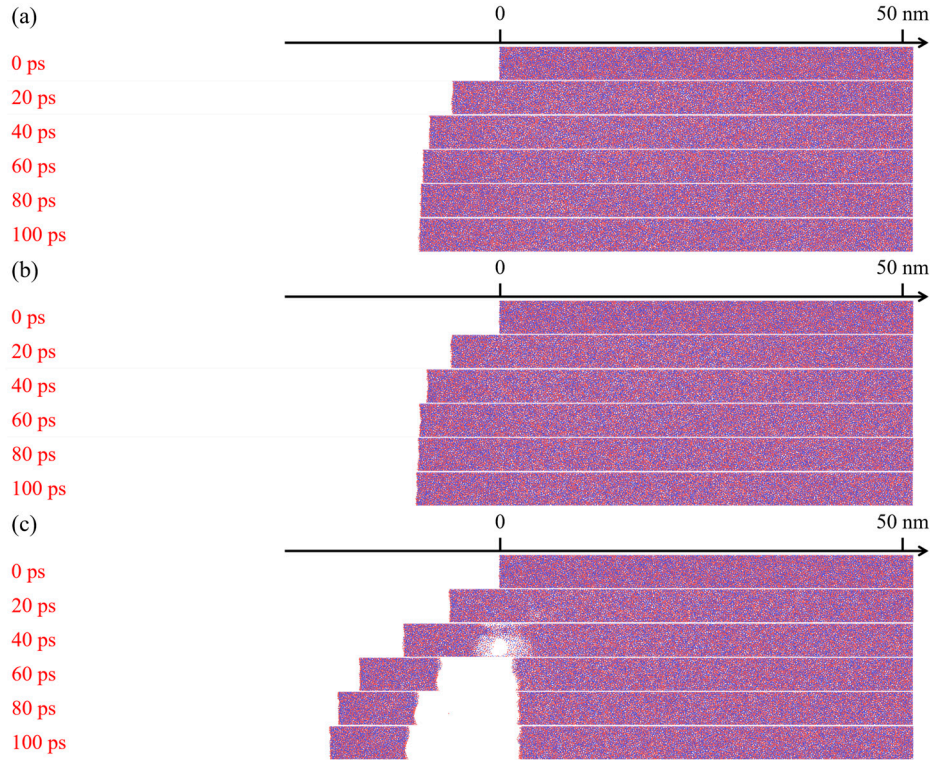

Figure 3. Snapshots (generated using the OVITO (Open Visualization Tool) software [35]) of $Cu_{50}Zr_{50}$ metallic glass irradiated by femtosecond laser with a pulse duration of 100 fs and absorbed fluence of (**a**) 80 mJ/cm^2, (**b**) 82 mJ/cm^2, and (**c**) 84 mJ/cm^2 from 0 to 100 ps. The laser pulse is incident from the left.

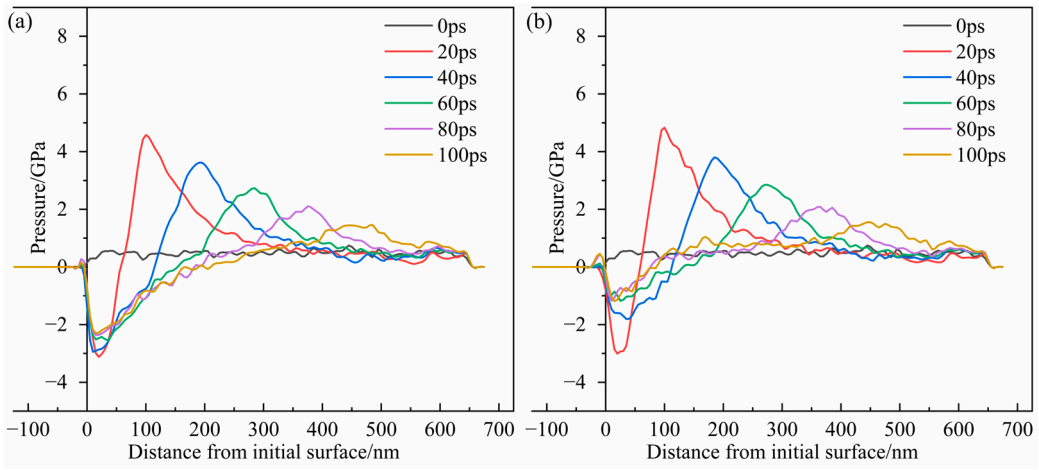

Figure 4. Spatial pressure profile for $Cu_{50}Zr_{50}$ metallic glass at different times and at absorbed fluence of (**a**) 80 mJ/cm^2 and (**b**) 84 mJ/cm^2. The initial surface is at position x = 0 nm.

3.2. Evolution of Femtosecond Laser Ablation at Different Fluences

To investigate the effects of different fluences on $Cu_{50}Zr_{50}$ metallic glass, laser pulses with a pulse duration of 100 fs and absorbed fluences of 90, 100, and 160 mJ/cm^2 were used to vertically irradiate the $Cu_{50}Zr_{50}$ metallic glass with a thickness of approximately 645 nm. The laser pulse was incident from left to right, and the snapshots of the target at different times are shown in Figure 5.

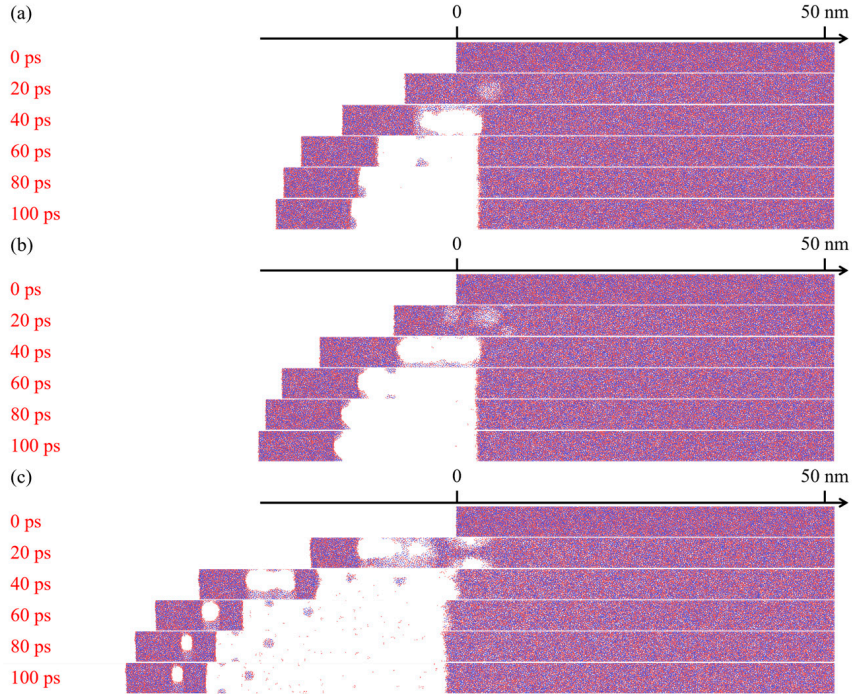

Figure 5. Snapshots of $Cu_{50}Zr_{50}$ metallic glass irradiated by femtosecond laser, with a pulse duration of 100 fs and absorbed fluences of (**a**) 90 mJ/cm^2, (**b**) 100 mJ/cm^2, and (**c**) 160 mJ/cm^2 from 0 to 100 ps. The laser pulse is incident from the left.

Figure 5 shows snapshots of the target after being irradiated by a single-pulse femtosecond laser with a pulse duration of 100 fs and absorbed fluence of 90~160 mJ/cm^2. At 20 ps, the targets at three laser conditions had already started to change. From 40 to 100 ps range, not only did the target material exhibit layer cracking, but large clusters of atoms were also produced, accompanied by violent phase explosions at the initial position of the target material. Moreover, it can be seen that an increasing number of single atoms and large clusters of atoms are ejected from the initial surface of the target material, causing the thickness of the ablated material to increase. If the pulse duration is the same, the target is more prone to ablation at the high absorbed fluence of the femtosecond laser.

According to Figure 6, the higher the absorbed fluence of the femtosecond laser, the more energy the target can absorb, and the electron temperature increases correspondingly. When the absorbed fluence is the same, after single-pulse femtosecond laser irradiation, the electron temperature in the absorption layer of the material decreases with the increase in depth, while the coupling time changes the opposite. The maximum electron temperatures of the initial target surface (x = 0 nm) after irradiation by femtosecond lasers with absorbed fluences of 90 mJ/cm^2, 100 mJ/cm^2, and 160 mJ/cm^2 were 8964 K, 9452 K, and 11,976 K, respectively. With the increase in the absorbed fluence, the maximum electron temperature gradually increases. This is mainly because under the condition of constant pulse duration, the increase in absorbed fluence represents the increase in peak power, thus causing the maximum electron temperature to rise. The reason why the highest electron temperature gradually increases with the increase in the absorbed fluence can be attributed to the following factors:

1. Increasing the absorbed fluence can increase the number of photons, which in turn improves the laser absorption rate and energy conversion efficiency. This promotes the absorption and conversion of energy into thermal energy in a more effective way.
2. More laser energy being absorbed into the material can lead to more excited electrons in a high-energy state, which results in an increase in electron temperature.
3. The increase in electron temperature can also lead to an increase in the thermal conductivity of the material, which accelerates the transfer of heat, causing the overall

material temperature to rise. This temperature increase may continue to occur during the reflux period, and the increase in electron temperature may be the result of complicated interactions between temperature and pressure.

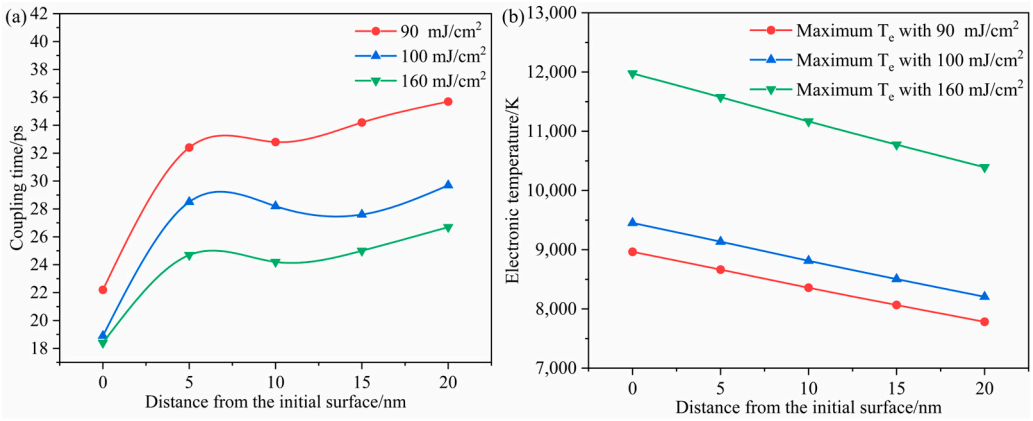

Figure 6. The variation of (**a**) the electron–lattice equilibrium temperature coupling time and (**b**) the maximum electronic temperature in the surface of $Cu_{50}Zr_{50}$ metallic glass irradiated by femtosecond laser irradiation, with a pulse duration of 100 fs and absorbed fluences of 90 mJ/cm^2, 100 mJ/cm^2, and 160 mJ/cm^2 depending on depth. The initial surface is at position x = 0 nm.

To investigate the cause of target fracture in $Cu_{50}Zr_{50}$ metallic glass under the loading of femtosecond lasers with a pulse duration of 100 fs and absorbed fluence of 90 mJ/cm^2, we analyzed the propagation of pressure inside the target material from 0 to 100 ps, as shown in Figure 7. The phenomenon of spallation is caused by the propagation of high-pressure compression waves generated near the surface of a target material. These waves reflect upon reaching the surface and create rarefaction waves that travel back into the bulk of the material. If the intensity of the rarefaction wave exceeds the strength of target, it can cause failure and the detachment of large pieces of matter near the surface. With the increase in time, the shock wave induced by the laser began to propagate deeper into the target material. The surface material underwent expansion and fracture between 0 ps and 100 ps due to the pressure on the surface of the target.

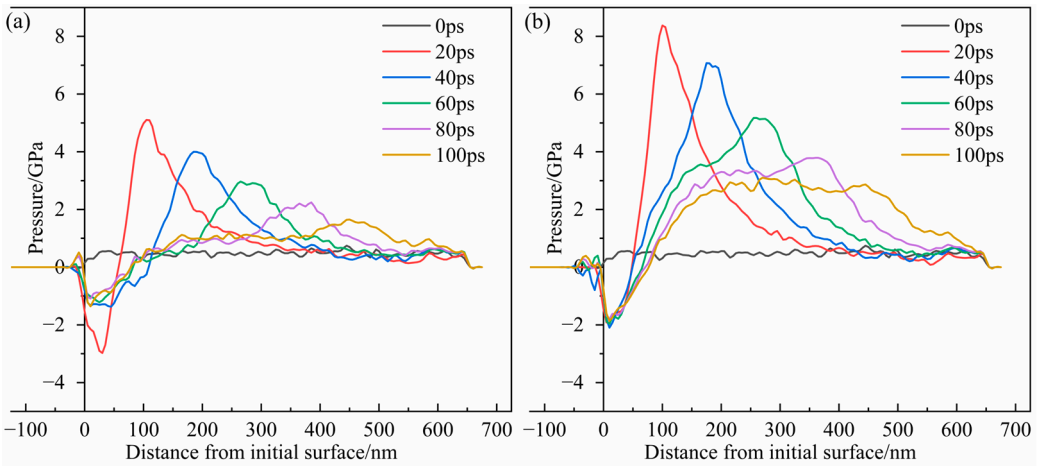

Figure 7. Spatial pressure profile for $Cu_{50}Zr_{50}$ metallic glass at different times and at absorbed fluences of (**a**) 90 mJ/cm^2 and (**b**) 160 mJ/cm^2. The initial surface is at position x = 0 nm.

3.3. Evolution of Femtosecond Laser Ablation at Different Pulse Durations

To investigate the effect of pulse durations on the femtosecond laser processing of metallic glass, $Cu_{50}Zr_{50}$ metallic glass with a thickness of approximately 645 nm was

irradiated by single-pulse femtosecond lasers with an absorbed fluence of 160 mJ/cm^2 and pulse durations of 50 fs, 100 fs, 200 fs, and 500 fs. The snapshots of the target at different times are shown in Figure 8. The laser incidence direction is from left to right.

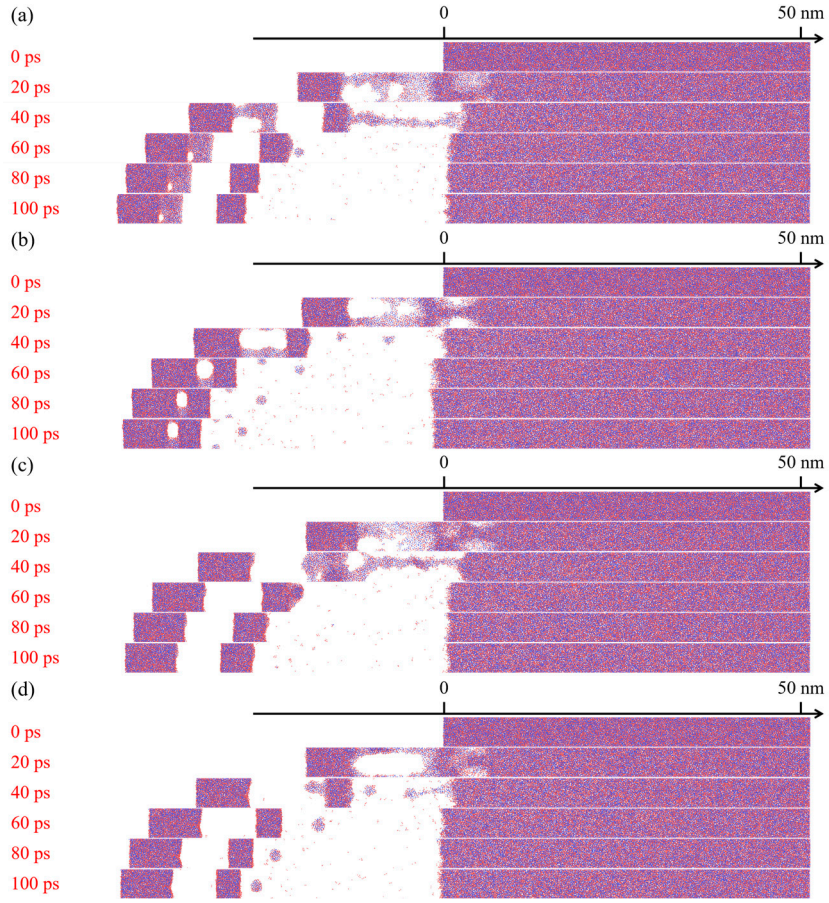

Figure 8. Snapshots of $Cu_{50}Zr_{50}$ metallic glass irradiated by femtosecond laser with absorbed fluence of 160 mJ/cm^2 and pulse durations of 50 fs (**a**), 100 fs (**b**), 200 fs (**c**), and 500 fs (**d**) from 0 to 100 ps. The laser pulse is incident from the left.

In Figure 8, when the absorbed fluence was 160 mJ/cm^2, the target material began to ablate at 20 ps, with the appearance of voids in the sub-surface of the target and the production of larger clusters of surface material dragged out by the expanding voids that led to target fracture. Between 40~60 ps, obvious laminations appeared in the target, with decreasing gaps between the layers; this was accompanied by more significant clusters of atoms being ablated from the target mother material. At 100 ps, ablation no longer occurred, and although the target material was partially removed, the subsurface region of the target material closer to the surface was occupied by thermal atoms that were emitted due to bottom-up thermal expansion.

Figure 9 shows the maximum electron temperature of the surface of the $Cu_{50}Zr_{50}$ metallic glass target, as well as the distribution of the electron–phonon coupling time with respect to space after irradiation with four pulse durations of 50 fs, 100 fs, 200 fs, and 500 fs, all with an absorbed fluence of 160 mJ/cm^2. From Figure 9a, it can be seen that increasing the pulse duration has no significant effect on the electron–lattice temperature coupling time of the target surface. From Figure 9b, it can be seen that the maximum electron temperature of the target surface decreases gradually with increasing depth. At the same position of the target, the maximum electron temperature decreases as the pulse duration increases. The maximum electron temperatures of the initial target surface (x = 0 nm) after

irradiation by femtosecond lasers with pulse durations of 50 fs, 100 fs, 200 fs, and 500 fs were 12,116 K, 11,976 K, 11,893 K, and 11,758 K, respectively.

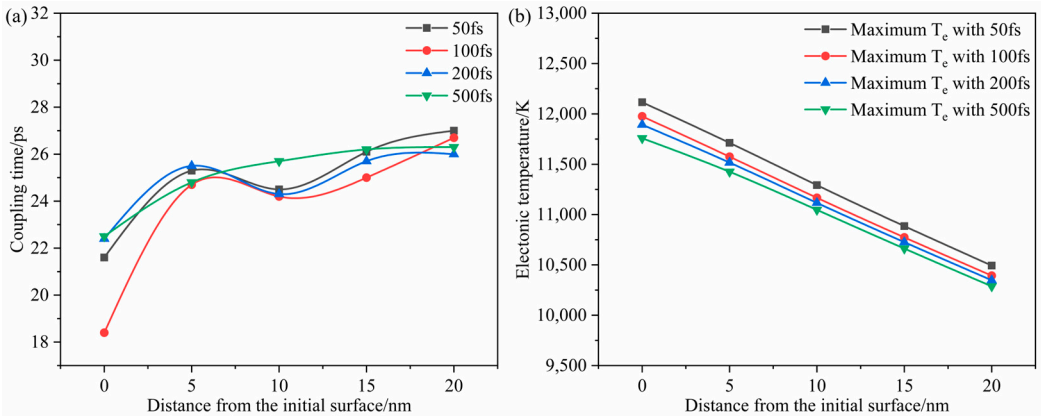

Figure 9. The variation of the electron–lattice equilibrium temperature coupling time (**a**) and the maximum electronic temperature (**b**) in the surface of $Cu_{50}Zr_{50}$ metallic glass irradiated by femtosecond laser irradiation, with absorbed fluence of 160 mJ/cm^2 and pulse durations of 50 fs, 100 fs, 200 fs, and 500 fs depending on depth. The initial surface is at position x = 0 nm.

As the pulse duration increases, the duration of femtosecond laser loading on $Cu_{50}Zr_{50}$ metallic glass tends to lengthen; thus, the time it takes for the electrons and lattice temperature to reach an equilibrium state also increases. With the increase in pulse duration, the highest electron temperature has a gradual downward trend. This is mainly because under the condition of constant pulse energy, the widening of pulse duration represents the decrease in peak power; thus, the highest electron temperature decreases.

4. Conclusions

In this paper, a hybrid TTM-MD approach was used to simulate the process of single-pulse femtosecond laser ablation of $Cu_{50}Zr_{50}$ metallic glass target material with a thickness of 644.9 nm, and the mechanisms underlying different absorbed fluences F_{abs} and pulse durations τ were analyzed.

1. It was determined that the ablation threshold of a target under $\tau = 100$ fs was 84 mJ/cm^2. Further, the tension near the surface decreased because it was "absorbed" by the cavities that finally caused ablation on the target material.
2. The process of the single-pulse femtosecond laser machining of $Cu_{50}Zr_{50}$ metallic glass was studied with $F_{abs} = 80, 82, 84, 90, 100, 160$ mJ/cm^2. As τ increased, the maximum T_e at the same position on the target surface decreased, while the $T_e - T_{ion}$ coupling time showed no significant difference. Further, it was found that the increase in F_{abs} leads to various forms of surface ablation on the target material, including melting, cavitation, spallation, material ejection, and phase explosion.
3. The mechanism between the femtosecond laser and metallic glass was researched by $\tau = 50, 100, 200, 500$ fs. It was found that the variation of τ had little effect on the electron–lattice temperature evolution, but it did have an impact on the structural changes during the ablation process. As the absorbed fluence increased, the maximum T_e at the same position on the target surface increased, while the $T_e - T_{ion}$ coupling time became shorter.

Author Contributions: Conceptualization, J.X. and S.X.; methodology, J.X. and Y.W.; validation, D.X. and O.G.; investigation, J.X. and D.X.; writing—original draft preparation, J.X. and D.X.; writing—review and editing, J.X., D.X., O.G., Y.W. and S.X.; supervision, J.X.; project administration, J.X.; funding acquisition, J.X. All authors have read and agreed to the published version of the manuscript.

Funding: This research was funded by the Young Eastern Scholar Program at Shanghai Institutions of Higher Learning and the Startup Foundation for Young Teachers of Shanghai Ocean University (No. A2-2006-00-200372).

Data Availability Statement: Data are contained within the article.

Acknowledgments: Support from the Young Eastern Scholar Program at Shanghai Institutions of Higher Learning is gratefully acknowledged. The project is also supported by the Startup Foundation for Young Teachers of Shanghai Ocean University (No. A2-2006-00-200372).

Conflicts of Interest: The authors declare no conflict of interest.

References

1. Wang, W. Brief History, Present and Future of Metallic Glasses. *Chin. J. Nat.* **2022**, *44*, 173–181.
2. Wu, Y.; Liu, X.; Lv, Z. A New Member of the Glass Family—Metallic Glass. *Physics* **2022**, *51*, 691–700.
3. Han, L.; Ming, P.; Kong, Z.; Zhang, X. Status and Research Progress of Metallic Glass Micro-Manufacturing Technology. *J. Netshape Form. Eng.* **2022**, *14*, 40–49.
4. Yao, Y.; Tang, J.; Zhang, Y.; Hu, Y.; Wu, D. Development of Laser Fabrication Technology for Amorphous Alloys. *Chin. J. Lasers* **2021**, *48*, 174–189.
5. Sano, T.; Takahashi, K.; Hirose, A.; Kobayashi, K.F. Femtosecond Laser Ablation of Zr55Al10Ni5Cu30 Bulk Metallic Glass. *Mater. Sci. Forum* **2007**, *539–543*, 1951–1954. [CrossRef]
6. Wang, X.; Lu, P.; Dai, N.; Li, Y.; Liao, C.; Zheng, Q.; Liu, L. Noncrystalline Micromachining of Amorphous Alloys Using Femtosecond Laser Pulses. *Mater. Lett.* **2007**, *61*, 4290–4293. [CrossRef]
7. Ma, F.; Yang, J.; Zhu, X.; Liang, C.; Wang, H. Femtosecond Laser-Induced Concentric Ring Microstructures on Zr-Based Metallic Glass. *Appl. Surf. Sci.* **2010**, *256*, 3653–3660. [CrossRef]
8. Anisimov, S.I.; Kapeliovich, B.L.; Perelman, T.L. Electron Emission from Metal Surfaces Exposed to Ultrashort Laser Pulses. *J. Exp. Theor. Phys.* **1974**, *66*, 375–377.
9. Perez, D.; Lewis, L.J. Ablation of Solids under Femtosecond Laser Pulses. *Phys. Rev. Lett.* **2002**, *89*, 255504. [CrossRef]
10. Lorazo, P.; Lewis, L.J.; Meunier, M. Short-Pulse Laser Ablation of Solids: From Phase Explosion to Fragmentation. *Phys. Rev. Lett.* **2003**, *91*, 225502. [CrossRef]
11. Perez, D.; Lewis, L.J. Molecular-Dynamics Study of Ablation of Solids under Femtosecond Laser Pulses. *Phys. Rev. B* **2003**, *67*, 184102. [CrossRef]
12. Smirnova, J.A.; Zhigilei, L.V.; Garrison, B.J. A Combined Molecular Dynamics and Finite Element Method Technique Applied to Laser Induced Pressure Wave Propagation. *Comput. Phys. Commun.* **1999**, *118*, 11–16. [CrossRef]
13. Kotake, S.; Kuroki, M. Molecular Dynamics Study of Solid Melting and Vaporization by Laser Irradiation. *Int. J. Heat Mass Transf.* **1993**, *36*, 2061–2067. [CrossRef]
14. Xie, J.; Yan, J.; Zhu, D. Atomic Simulation of Irradiation of Cu Film Using Femtosecond Laser with Different Pulse Durations. *J. Laser Appl.* **2020**, *32*, 022016. [CrossRef]
15. Förster, G.D.; Lewis, L.J. Numerical Study of Double-Pulse Laser Ablation of Al. *Phys. Rev. B* **2018**, *97*, 224301. [CrossRef]
16. Ivanov, D.S.; Zhigilei, L.V. Combined Atomistic-Continuum Modeling of Short-Pulse Laser Melting and Disintegration of Metal Films. *Phys. Rev. B* **2003**, *68*, 064114. [CrossRef]
17. Yuan, W.; Sizyuk, T. Ablation Study in Gold Irradiated by Single Femtosecond Laser Pulse with Electron Temperature Dependent Interatomic Potential and Electron–Phonon Coupling Factor. *Laser Phys.* **2021**, *31*, 036002. [CrossRef]
18. Marinier, S.; Lewis, L.J. Femtosecond Laser Ablation of CuxZr1-x Bulk Metallic Glasses: A Molecular Dynamics Study. *Phys. Rev. B Condens. Matter Mater. Phys.* **2015**, *92*, 184108. [CrossRef]
19. Iabbaden, D.; Amodeo, J.; Fusco, C.; Garrelie, F.; Colombier, J.P. Molecular Dynamics Simulation of Structural Evolution in Crystalline and Amorphous CuZr Alloys upon Ultrafast Laser Irradiation. *Phys. Rev. Mater.* **2022**, *6*, 126001. [CrossRef]
20. Plimpton, S. Fast Parallel Algorithms for Short-Range Molecular Dynamics. *J. Comput. Phys.* **1995**, *117*, 1–19. [CrossRef]
21. Chen, J.K.; Tzou, D.Y.; Beraun, J.E. A Semiclassical Two-Temperature Model for Ultrafast Laser Heating. *Int. J. Heat Mass Transf.* **2006**, *49*, 307–316. [CrossRef]
22. Falkovsky, L.A.; Mishchenko, E.G. Electron-Lattice Kinetics of Metals Heated by Ultrashort Laser Pulses. *J. Exp. Theor. Phys.* **1999**, *88*, 84–88. [CrossRef]
23. Choy, C.L.; Tong, K.W.; Wong, H.K.; Leung, W.P. Thermal Conductivity of Amorphous Alloys above Room Temperature. *J. Appl. Phys.* **1991**, *70*, 4919–4925. [CrossRef]
24. Mendelev, M.I.; Kramer, M.J.; Ott, R.T.; Sordelet, D.J.; Yagodin, D.; Popel, P. Development of Suitable Interatomic Potentials for Simulation of Liquid and Amorphous Cu–Zr Alloys. *Philos. Mag.* **2009**, *89*, 967–987. [CrossRef]
25. Daw, M.S.; Baskes, M.I. Embedded-Atom Method: Derivation and Application to Impurities, Surfaces, and Other Defects in Metals. *Phys. Rev. B* **1984**, *29*, 6443–6453. [CrossRef]
26. Finnis, M.W.; Sinclair, J.E. A Simple Empirical *N*-Body Potential for Transition Metals. *Philos. Mag. A* **1984**, *50*, 45–55. [CrossRef]

27. Zhu, P.; Fang, F. On the Mechanism of Material Removal in Nanometric Cutting of Metallic Glass. *Appl. Phys. A* **2014**, *116*, 605–610. [CrossRef]
28. Murali, P.; Guo, T.F.; Zhang, Y.W.; Narasimhan, R.; Li, Y.; Gao, H.J. Atomic Scale Fluctuations Govern Brittle Fracture and Cavitation Behavior in Metallic Glasses. *Phys. Rev. Lett.* **2011**, *107*, 215501. [CrossRef]
29. Shugaev, M.V.; He, M.; Levy, Y.; Mazzi, A.; Miotello, A.; Bulgakova, N.M.; Zhigilei, L.V. Laser-Induced Thermal Processes: Heat Transfer, Generation of Stresses, Melting and Solidification, Vaporization, and Phase Explosion. In *Handbook of Laser Micro- and Nano-Engineering*; Springer International Publishing: Cham, Switzerland, 2020; pp. 1–81.
30. Shugaev, M.V.; Zhigilei, L.V. Thermoelastic Modeling of Laser-Induced Generation of Strong Surface Acoustic Waves. *J. Appl. Phys.* **2021**, *130*, 185108. [CrossRef]
31. Available online: https://docs.lammps.org/fix_viscous.html (accessed on 1 March 2023).
32. Zhigilei, L.V.; Lin, Z.; Ivanov, D.S. Atomistic Modeling of Short Pulse Laser Ablation of Metals: Connections between Melting, Spallation, and Phase Explosion. *J. Phys. Chem. C* **2009**, *113*, 11892–11906. [CrossRef]
33. Schäfer, C.; Urbassek, H.M.; Zhigilei, L.V. Metal Ablation by Picosecond Laser Pulses: A Hybrid Simulation. *Phys. Rev. B* **2002**, *66*, 115404. [CrossRef]
34. Hu, Y.; Jiang, G. Study on the Damage Dynamics of CuZr Amorphous Alloy Nanofilm Irradiated by Femtosecond Laser. *J. Sichuan Univ. Nat. Sci. Ed.* **2019**, *56*, 897–902.
35. Stukowski, A. Visualization and Analysis of Atomistic Simulation Data with OVITO–the Open Visualization Tool. *Model. Simul. Mater. Sci. Eng.* **2010**, *18*, 015012. [CrossRef]

Disclaimer/Publisher's Note: The statements, opinions and data contained in all publications are solely those of the individual author(s) and contributor(s) and not of MDPI and/or the editor(s). MDPI and/or the editor(s) disclaim responsibility for any injury to people or property resulting from any ideas, methods, instructions or products referred to in the content.